The Endophilin N-BAR Domain Perturbs the Structure of Lipid Bilayers

ARTICLE *in* BIOCHEMISTRY · JULY 2010

Impact Factor: 3.02 · DOI: 10.1021/bi100760e · Source: PubMed

2 AUTHORS, INCLUDING:

Swetha Suresh
University of Cambridge
5 PUBLICATIONS **59** CITATIONS

5766 *Biochemistry* **2010,** *49,* 5766–5771
DOI: 10.1021/bi100760e

BIOCHEMISTRY
including biophysical chemistry & molecular biology
Article

The Endophilin N-BAR Domain Perturbs the Structure of Lipid Bilayers†

Swetha Suresh and J. Michael Edwardson*

Department of Pharmacology, University of Cambridge, Cambridge CB2 1PD, United Kingdom

Received May 13, 2010; Revised Manuscript Received June 3, 2010

ABSTRACT: Endophilin A is a key player in clathrin-mediated endocytosis at nerve terminals and is essential for the maintenance of synaptic transmission. Endophilin consists of two regions: an SH3 domain that interacts with other endocytotic proteins and an N-BAR domain that binds and bends membranes. Here, we used atomic force microscopy (AFM) under fluid to examine the interaction of the endophilin N-BAR domain with planar supported lipid bilayers, under conditions that closely mimic the environment in which this protein normally operates. We found that when bound to lipid bilayers, the N-BAR domain formed aggregates of various sizes. The N-BAR domain also perturbed the structure of the planar bilayer, at a low concentration (0.15 μM) causing bilayer thinning, and at a 10-fold higher concentration (1.5 μM) forming thin slivers from the bilayer sheet. This bilayer sculpting effect crucially involved the central appendage domain. Reduced hydrophobicity in this domain, caused by the A66D mutation, almost abolished the ability of the endophilin N-BAR domain to bind to supported bilayers. In contrast, increased hydrophobicity, caused by the A66W mutation, switched the bilayer sculpting effect of the N-BAR domain from sliver formation to vesiculation. By following the action of the endophilin N-BAR domain under near-physiological conditions, we have been able to provide additional insights into its membrane binding and bending mechanism.

Synaptic vesicle recycling by clathrin-mediated endocytosis is crucial to the maintenance of neurotransmission at synapses (reviewed in refs *1* and *2*). There is ample evidence that endophilin A1, a 40 kDa cytosolic protein that is enriched in nerve terminals, is a key player in clathrin-mediated endocytosis (*3*). For instance, in *Drosophila* and *Caenorhabditis elegans*, endophilin mutants have defective synaptic recycling (*4*−*6*), and injection of an anti-endophilin antibody into the nerve terminal of the giant lamprey reticulospinal synapse causes the accumulation of a large number of clathrin-coated structures without constricted necks, and shallow pits (*7*). Further, when endophilin is depleted from brain cytosol by immunoadsorption, the number of endocytotic structures is reduced 8-fold (*7*).

Endophilin has two domains, an N-BAR domain [residues 1−247 in the human form of the protein (*8*)] and an SH3 domain [residues 290−345 (*9*, *10*)]. The BAR domain[1] is structurally similar to the N-terminal region of Bin, amphiphysin, and Rvs 161/167 (*11*). This domain is responsible for endophilin dimerization and for membrane binding and bending (*8*, *12*−*15*). The SH3 domain recruits other endocytotic proteins, such as dynamin and synaptojanin, by binding to their proline-rich regions (*10*, *16*, *17*). The endophilin A1 N-BAR domain has been crystallized in the form of a dimer, which has a crescent-shaped structure, suggestive of the mechanism by which it binds membranes (*13*−*15*).

Endophilin interacts electrostatically with membranes and, in vitro, is able to induce tubulation and vesiculation of liposomes (*14*, *15*). Each monomer forms a coiled-coil structure with three bundles of antiparallel helices. Endophilin has a conserved N-terminal region that is disordered in the crystal structure but forms an α-helix on contact with the membrane (*14*, *15*). This region is essential for membrane binding. The endophilin dimer is concave and rigid, and able to act as a scaffold, impressing its shape on the membrane either to sense or to drive curvature. The charge distribution over the surface of the dimer is highly asymmetric, with the concave face being positively charged and the convex face negatively charged (*13*−*15*). Clearly, the positive charges on the concave face will aid in the binding of the protein to a negatively charged lipid bilayer. The endophilin BAR structure also has an appendage (residues 59−88) protruding from the center of the dimer (*14*, *15*). Except for a small number of conserved hydrophobic amino acids, the residues in the appendage are distinct between the endophilin A and B families. The appendage is able to penetrate the membrane, thereby promoting tubulation of liposomes (*18*). Introduction of a negative charge into this region, as in the mutant A66D, abolishes tubulation, while introduction of a bulky hydrophobic residue, as in A66W, causes liposome vesiculation in addition to tubulation (*14*). Interestingly, neither of these mutations affects the binding of endophilin to liposomes.

When the endophilin N-BAR domain was crystallized, it was found to coordinate 11 Cd^{2+} ions (*13*). Since the ionic radii of Ca^{2+} and Cd^{2+} are similar (0.97 and 0.99 Å, respectively), endophilin was suggested to bind Ca^{2+} under physiological conditions. This idea was consistent with previous evidence for a Ca^{2+}-dependent interaction of endophilin with voltage-gated Ca^{2+} channels (*19*). However, isothermal titration calorimetry produced no evidence that Ca^{2+} binds to the endophilin N-BAR domain, and the protein did not compete for Ca^{2+} with dibromo BAPTA (*15*).

In the past, imaging of the interaction of endophilin with lipids has been restricted to electron microscopy (EM), which

†S.S. is supported by a Cambridge Nehru Fellowship and a Cambridge Overseas Research Studentship.

*To whom correspondence should be addressed. Phone: 44-1223-334014. Fax: 44-1223-334100. E-mail: jme1000@cam.ac.uk.

[1]Abbreviations: AFM, atomic force microscopy; BAR domain, Bin, amphiphysin, and Rvs domain; DOPC, 1,2-dioleoyl-*sn*-glycero-3-phosphocholine; DOPE, 1,2-dioleoyl-*sn*-glycero-3-phosphoethanolamine; DOPS, 1,2-dioleoyl-*sn*-glycero-3-phosphoserine; EM, electron microscopy; HBS, Hepes-buffered saline.

 Published on Web 06/08/2010

necessarily involves the use of highly processed, dried samples (*12*, *14*, *15*). Further, the liposomes to which the endophilin has been bound have, of course, had a significant positive curvature, unlike the situation in the presynaptic terminal where the membrane is effectively planar. Atomic force microscopy (AFM) enables the imaging of interactions of the protein with planar lipid bilayers under near-physiological conditions (i.e., under fluid). For example, we have used AFM to follow changes in the structure of bilayers containing sphingomyelin/cholesterol-rich domains ("rafts") in response to manipulation of cholesterol levels (*20*), to examine the lateral organization of proteins in raft-containing bilayers (e.g., ref *21*), and to visualize the perturbation of bilayer structure caused by the binding of synaptotagmin, the Ca^{2+} sensor for neuronal exocytosis (*22*). In this study, we have used AFM to show that the endophilin A1 N-BAR domain profoundly perturbs the structure of lipid bilayers. We also show that the A66W and A66D mutations significantly affect the protein−bilayer interaction.

EXPERIMENTAL PROCEDURES

Expression and Purification of Proteins. The mouse endophilin A1 N-BAR domain (residues 1−247; wild type and mutants A66W and A66D) was expressed in the pET-28a vector (Novagen), which adds an N-terminal His_6 tag. The constructs were transformed into BL21 DE3 *Escherichia coli* (Invitrogen). Expressed proteins were affinity purified on Probond Ni^{2+}-agarose resin (Invitrogen) and eluted with 400 mM imidazole. The yield of the N-BAR domain was 0.5−1 mg/L of culture. The His_6 tags were cleaved from the eluted proteins by incubation with 5 units/mL thrombin (Amersham Biosciences) for 12 h at room temperature, and the thrombin was removed using benzamidine beads (GE Healthcare). Protein purity was checked by SDS−PAGE followed by Coomassie blue staining. Immunoblotting using an anti-His_6 antibody (Invitrogen) was used to confirm the complete cleavage of the tag. Purified proteins were either used immediately or stored as frozen aliquots at −80 °C.

Atomic Force Microscopy. AFM imaging was performed using a Veeco Digital Instruments Multimode instrument, controlled by a Nanoscope IIIa controller. Imaging in air was conducted using Si probes (OMCL-AC160TS-E, Olympus), which have a resonance frequency of 300 kHz. Imaging under fluid was conducted using NSC-18 cantilevers with a Cr−Au coating (Mikromasch). Their resonant frequencies were 30−35 kHz, and the actual scanning frequencies were ∼5% below the maximal resonance peak. In both cases, the root-mean-square voltage was maintained at 2 V.

Imaging of Protein on Mica. Protein was diluted to 1 μg/mL (33 nM) in Hepes-buffered saline (HBS) [50 mM Hepes (pH 7.6) and 150 mM NaCl] containing 1 mM Ca^{2+}, and 50 μL was placed on freshly cleaved mica (Ca^{2+} was added to the buffer solution in an attempt to mimic conditions during Ca^{2+}-triggered neurotransmitter release at the presynaptic terminal). After a 20 min incubation, samples were washed with 10 mL of ultrapure water (BPC grade, Sigma-Aldrich) to remove unadsorbed protein. All imaging was conducted at room temperature. Experiments were conducted three times, using independent protein preparations.

Imaging of Proteins on Lipid Bilayers. 1,2-Dioleoyl-*sn*-glycero-3-phosphocholine (DOPC), 1,2-dioleoyl-*sn*-glycero-3-phosphoethanolamine (DOPE), and 1,2-dioleoyl-*sn*-glycero-3-phosphoserine (DOPS) were purchased as chloroform solutions from Avanti Polar Lipids. Lipid mixtures containing DOPC and DOPS or DOPC and DOPE (molar ratio of 3:1) were dried under nitrogen and hydrated in water overnight at 4 °C. Lipid suspensions were vortexed and then probe-sonicated at an amplitude of 10 μA for 5−10 s until the mixture became transparent. The suspensions were incubated on ice for 10−15 min before the formation of bilayers. Liposomes (50 μL) were placed on freshly cleaved mica along with 50 μL of HBS containing 1 mM $CaCl_2$ and left for 6 min. The mica was washed twice with 1 mL of the same buffer and immediately placed in the fluid cell of the atomic force microscope. The mounted bilayer was immersed in 150 μL of HBS containing 0.5 mM $CaCl_2$. All imaging was conducted at room temperature. Routinely, bilayers were first imaged before the addition of protein, as a control. Proteins were diluted to the appropriate final concentration (either 0.15 or 1.5 μM) in imaging buffer (above), and this was exchanged with the protein-free buffer in the fluid cell.

Data Analysis. All AFM images were plane-fitted before any analysis to remove tilt. Since the scan sizes used for particle analysis were either 1 or 2 μm square, the plane fit order used was 1. Each scan line used to make up the image was therefore fitted to a first-order equation, and loss of data was minimal. For dry imaging, particles were analyzed using the NanoscopeV5.31rl software. Fifty particles were first analyzed manually. These measurements were used to define the detection level in the program, which in turn defines the minimum z value to be considered as part of the particle. After particles were thus defined, the height and radius (radius of a circle fitted to data obtained for each particle) were determined. For fluid imaging, particles were first identified from the phase image and their heights and radii were measured manually using the section tool.

Bound particles assumed the approximate shape of a spherical cap. The radius and height of each particle were used to calculate its molecular volume using the formula

$$V_m = (\pi h/6)(3r^2 + h^2) \quad (1)$$

where h is the particle height and r is the radius, as described previously (*23*). For comparison, molecular volume based on molecular mass was calculated using the equation

$$V_c = (M_0/N_0)(V_1 + dV_2) \quad (2)$$

where M_0 is the molecular mass, N_0 is Avogadro's number, V_1 and V_2 are the partial specific volumes of the particle (0.74 cm^3/g) and water (1 cm^3/g), respectively, and d is the extent of protein hydration (taken as 0.4 g of water/g of protein).

Recently, we imaged (in air) a range of proteins of known molecular mass. We found a very good correlation between measured volumes and volumes expected on the basis of molecular mass (*24*). It has also been shown that protein volumes measured in air and under fluid are very similar, indicating that little protein dehydration occurs under the conditions used for air imaging (*25*). It is therefore reasonable to compare molecular volumes of the endophilin N-BAR domain determined in air and under fluid, as we do in this study.

RESULTS

Initially, the endophilin N-BAR domain was imaged when bound to mica. Protein was added to the mica at a concentration of 33 nM in HBS containing 1 mM Ca^{2+}, followed by drying and imaging in air, using tapping-mode AFM. A homogeneous population of particles was observed (Figure 1A). The radii

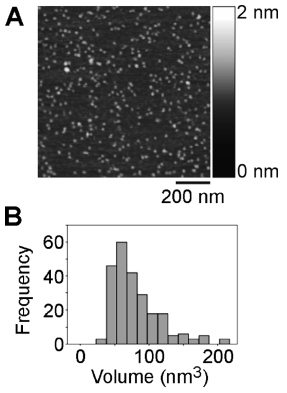

FIGURE 1: Interaction of the endophilin N-BAR domain with mica. Representative AFM image (A) and frequency distribution of particle volumes (B) for the endophilin N-BAR domain incubated at a concentration of 33 nM with mica in HBS containing 1 mM Ca^{2+}. Particle volumes were calculated using eq 1, assuming that they adopted the shape of a spherical cap. A shade−height scale is shown at the right.

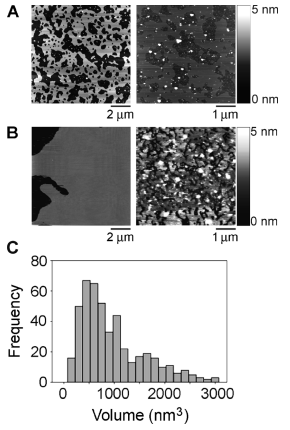

FIGURE 2: Interaction of the endophilin N-BAR domain, at a low concentration (0.15 μM), with supported lipid bilayers. (A) The left panel shows an AFM image of a protein-free bilayer composed of DOPC and DOPE (3:1). The right panel shows the same bilayer after addition of the endophilin N-BAR domain. Most of the protein bound to the mica. A shade−height scale is shown at the right. (B) The left panel shows a protein-free bilayer composed of DOPC and DOPS. The right panel shows the same bilayer after addition of the endophilin N-BAR domain. The protein bound as aggregates to the lipid bilayer. (C) Frequency distribution of molecular volumes for the endophilin N-BAR domain bound to bilayers.

and heights of a number of the particles were determined, and their volumes were calculated using eq 1, assuming that the particles adopted the shape of a spherical cap. The frequency distribution of molecular volumes (Figure 1B) had a peak at 60 nm^3. The predicted volume of an endophilin N-BAR domain monomer (molecular mass of 31 kDa) is 62 nm^3; hence, the measured volume suggests that under these conditions the N-BAR domain is predominantly monomeric. This is to be expected, given that the dissociation constant for endophilin N-BAR domain dimerization, determined using equilibrium ultracentrifugation, is 10 μM (*15*), considerably higher than the concentration used in the experiments.

Next the endophilin N-BAR domain was introduced onto supported lipid bilayers of different compositions [DOPC/DOPE (3:1) and DOPC/DOPS (3:1)], and the samples were imaged using AFM under fluid in HBS containing 0.5 mM Ca^{2+} (Figure 2). Before the addition of protein, the bilayers were almost featureless, and gaps in the bilayers revealed the underlying mica substrate (Figure 2A,B, left panels). When the endophilin N-BAR domain (0.15 μM) was added to the DOPC/DOPE bilayers, the majority of the particles associated with the mica and not the bilayer (Figure 2A, right panel). However, when DOPC/DOPS bilayers were used, many particles were seen on the bilayer surface (Figure 2B, right panel). Hence, for all further experiments, DOPC/DOPS bilayers were used as the model membrane. Analysis of protein volumes (Figure 2C) indicated that the protein associated with the bilayer as aggregates of varying stoichiometry. The peak of the frequency distribution of volumes was at 474 nm^3, considerably greater than the value of 60 nm^3 for the endophilin N-BAR domain bound to mica.

A typical bilayer had a measured height of 2.14 nm above the mica substrate (Figure 3A). This is smaller than the value expected for a bilayer of this lipid composition [~4 nm (reviewed in ref *26*)]. In fact, we have found recently that the measured bilayer thickness depends on the AFM probe used in the experiment. A direct comparison was made of the apparent bilayer thickness measured using a Veeco DNP-S silicon nitride probe and a Mikromasch NSC18 etched silicon probe, of the type used in this study. A thickness of 4 nm was seen with the Veeco probe, as previously reported (*20*−*22*), whereas the Mikromasch probe gave an apparent thickness of 2.5 nm. We suggest that this discrepancy may be caused by partial penetration of the bilayer

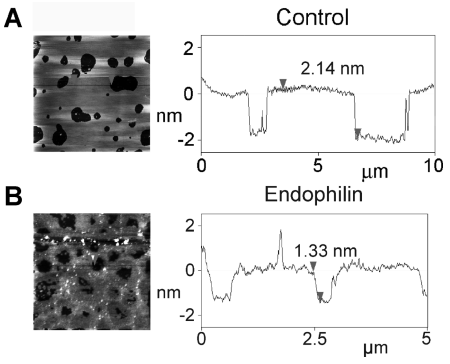

FIGURE 3: Effect of the endophilin N-BAR domain, at a low concentration, on bilayer thickness. AFM images of bilayers in the absence (A) and presence (B) of 0.15 μM endophilin N-BAR domain. The sections taken along the lines indicated show the bilayer thickness in the two cases.

by the Micromasch probe, which has a much stiffer spring constant (3.5 N/m) than the Veeco probe (0.58 N/m). Interestingly, at a low concentration (0.15 μM), the endophilin N-BAR domain caused an apparent thinning of the bilayer, as illustrated in Figure 3B. The surface of the bilayer is now less smooth than that seen in the absence of endophilin, and the height of the bilayer above the mica substrate is 1.33 nm. This membrane thinning effect was seen previously when bilayers were incubated with various antimicrobial peptides (*27*−*30*). At low concentrations, these peptides insert into the headgroup region of the bilayer in the form of amphipathic α-helices.

When a 10-fold higher concentration of endophilin was used (1.5 μM), the protein initially (0−5 min) acted on the lipid bilayers to form islands studded with protein (Figure 4A). At later times (10−15 min), the structure of the bilayer became dramatically altered. Specifically, the bilayer became extensively fenestrated, and thin slivers were pulled away from the main bilayer areas (Figure 4B). Later still (40−60 min), the bilayer began to reorganize itself, and the slivers were no longer visible, indicating that a "healing" process was underway. Note that

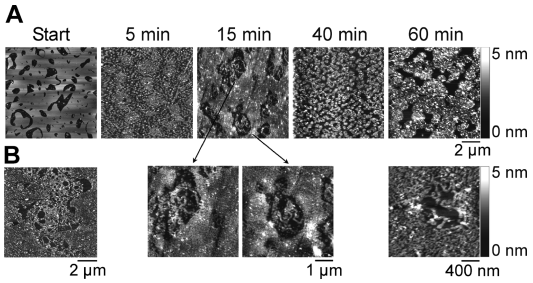

FIGURE 4: Bilayer sculpting effect of the endophilin N-BAR domain, at a high concentration. (A) AFM images of lipid bilayers taken various times after addition of the endophilin N-BAR domain (1.5 μM). A shade−height scale is shown at the right. Note that the left image, labeled Start, was obtained immediately before protein addition. (B) Further examples, at various magnifications, of bilayers, showing the fenestration and sliver formation caused by a 15 min incubation with the endophilin N-BAR domain (1.5 μM).

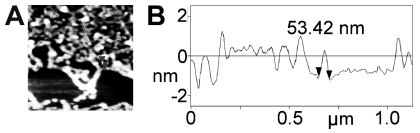

FIGURE 5: (A) Zoomed image illustrating sliver formation. The image was taken after incubation of the bilayer with the endophilin N-BAR domain for 15 min. (B) Profile of a sliver. The section was taken at the position indicated by the line in the AFM image.

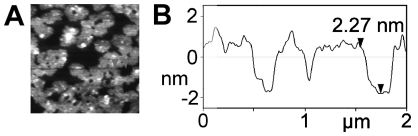

FIGURE 6: (A) AFM image illustrating bilayer healing. The image was taken after incubation with the endophilin N-BAR domain for 40 min. (B) Profile of the bilayer. The section was taken at the position indicated by the line in the AFM image.

repetitive scanning of protein-free bilayers did not significantly perturb bilayer structure (data not shown).

The structure of the bilayer slivers seen after a 15 min exposure of the bilayer to the endophilin N-BAR domain is illustrated in more detail in Figure 5A. A section through the slivers (Figure 5B) shows that they are ~1.5 nm high and 40−150 nm wide. The sections also reveal the roughness of the bilayer surface, in contrast to the smooth appearance of protein-free bilayers (Figure 2). During the period of bilayer healing, the slivers merged together (Figure 6A) and formed an intact bilayer studded with protein. The bilayer thickness returned to its control value of ~2.2 nm, despite the continued presence of bound protein particles (Figure 6B).

Mutations in the central appendage of the endophilin N-BAR domain have been shown previously to significantly affect the behavior of the protein. In particular, the A66D mutation abolished the ability of the endophilin N-BAR domain to tubulate liposomes, whereas the A66W mutation reduced the level of tubulation and caused vesiculation (*14*). When we examined the effect of the A66D mutant on lipid bilayers (after a 15 min incubation), we found that the protein associated preferentially with the mica substrate rather than the lipid bilayer (Figure 7A). In contrast, the A66W mutant acted as a "super-endophilin", forming the characteristic bilayer slivers at 15 min (Figure 7B, center two panels), but going on after 40 min to convert these slivers into small vesicles with diameters of 100−200 nm and

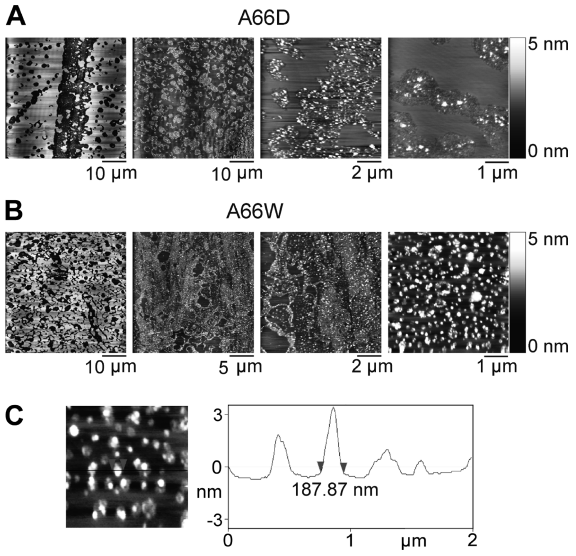

FIGURE 7: Effect of mutations in the central appendage on bilayer sculpting by the endophilin N-BAR domain. (A and B) AFM images of bilayers in the presence of either the A66D (A) or A66W (B) endophilin N-BAR domain mutant (1.5 μM). The left panel in each case shows a bilayer before the addition of protein. The other panels show bilayers imaged at various magnifications. Bilayers were exposed to protein for 15 min, except for the right panel in section B, where the incubation time was 40 min. Shade−height scales are shown at the right. (C) AFM image of vesicles produced by exposure of a bilayer to the A66W mutant. The section was taken at the position indicated by the line in the AFM image.

variable heights (Figure 7B, right panel), bearing bound protein (Figure 7C).

DISCUSSION

The ability of the endophilin N-BAR domain to tubulate bilayers has been demonstrated previously using EM (*12*, *14*, *15*); however, EM requires extensive sample processing and imaging under vacuum. Here, we have used AFM, which permits image acquisition under fluid, to investigate the process of remodeling of lipid bilayers by the endophilin N-BAR domain.

In our initial experiments, we visualized the endophilin N-BAR domain in association with mica. We found that the endophilin N-BAR domain bound to mica in the form of monomers. This observation suggests that at a concentration of 33 nM the endophilin N-BAR domain is monomeric in solution, consistent with a previous report that the dissociation constant for dimerization is 10 μM (*15*). In neurons, endophilin is present at an overall concentration of 0.1 μM, and this concentration is believed to increase by 10-fold in the presynaptic terminals (*15*). Our result therefore suggests that endophilin exists in monomeric form in the neuronal cytoplasm.

In the absence of DOPS, the protein bound mainly to mica. When the endophilin N-BAR domain was added to DOPS-containing lipid bilayers, the protein bound to the bilayer in the form of aggregates. This PS-dependent binding of the N-BAR domain to the bilayer is probably recapitulated in the neuron, where PS is localized to the inner leaflet of the presynaptic membrane. Because the protein in solution, at a free concentration of 0.15 μM [well below the 10 μM dissociation constant for dimerization (*15*)], is likely still to be primarily monomeric, our results suggest that the monomers land on the bilayer and then associate with each other. In the absence of DOPS, endophilin N-BAR domain multimers might still form on the bilayer and

then become displaced and bind instead to the mica substrate. This behavior would explain the presence of particles larger than those observed by dry imaging on mica. The lipid binding and self-association of the endophilin N-BAR domain likely involve the N-terminal amphipathic helix. It has been shown previously that a peptide mimicking the N-terminal helix binds strongly to anionic lipids and weakly to zwitterionic lipids. This peptide also oligomerizes in the presence of lipids (*31*). Cross-linking experiments with the full-length endophilin N-BAR domain have also shown that it oligomerizes in the presence of liposomes (*12*). We have been able to quantify the extent of oligomerization on lipid bilayers. There was a large spread of measured molecular volumes, but a prominent peak was observed at ~474 nm^3, indicating that the predominant oligomer contains approximately eight monomers (monomer volume of 60 nm^3).

At a low protein concentration, the endophilin N-BAR domain caused a significant thinning of the bilayer. This membrane thinning effect has been seen previously when bilayers were incubated with various antimicrobial peptides, such as magainin (*27*), alamethicin (*28*, *29*), and MSI-78 (*30*). At low concentrations, these peptides, each of which is ~20 amino acids long, insert into the headgroup region parallel to the plane of the bilayer, in the form of amphipathic α-helices. The peptides push the lipid molecules in the top monolayer apart, leading to tilting of the lipid chains. This causes a change in lipid packing, leading to membrane thinning over a relatively wide area. The fact that the N-terminal region of the endophilin N-BAR domain is similar in size to these peptides, and also interacts with the lipid headgroups in the form of an amphipathic α-helix (*15*), points to a similar mechanism of interaction with the bilayer. Interestingly, the bilayer thinning effect of the peptides mentioned above occurred only at low peptide concentrations (*27*−*30*). At higher concentrations, the peptides assembled into multimers, in which the individual peptides were perpendicular to the plane of the bilayer. In some cases, the multimers formed pores in the bilayer (e.g., ref *27*). It is tempting to speculate that a similar concerted action occurs with the endophilin N-BAR domain at higher concentrations. The aggregation might then trigger the rearrangement of the bilayer-penetrating regions of the protein, leading to the observed bilayer sculpting effects.

At a 10-fold higher concentration (1.5 μM), the endophilin N-BAR domain caused a sequence of changes in bilayer structure. Initially, binding occurred, and aggregates were formed. Then, the bilayer became extensively fenestrated, and slivers were peeled away from the main bilayer sheets. The majority of slivers formed had a width of 40−150 nm. The action of the N-BAR domain resulted in a reticulated or complex weblike structure, as predicted by mesoscopic simulations (*32*, *33*). The slivers generated are likely analogous to the tubules formed when the endophilin N-BAR domain acts on liposomes. The width of the slivers is comparable to the width of the neck of the vesicles. All-atom molecular dynamics simulations of the action of the N-BAR domain dimer of amphiphysin on lipid bilayers show that it can induce local membrane curvature (*34*). Subsequent coarse-grained simulations of amphiphysin N-BAR domain lattices (*35*, *36*) support the experimental observation that the type of lattice formed by the protein determines how much membrane curvature is generated (*37*). The range of widths of the slivers seen in our experiments might reflect the same process. Simulations show that bilayer bending first begins at the edges and then propagates to the center, proceeding to rounding up of the membrane and eventually to the formation of a tubule (*36*). This rounding up might be obstructed in our experiments, because of the firm attachment of the bilayer to the mica surface.

Eventually, the slivers disappeared and the bilayer "healed" itself. This type of behavior has been proposed for the amphiphysin N-BAR domain at a high density (*36*). When many N-BAR domains are clustered together, the N-terminal amphipathic helices should interact with each other and occlude interaction with the membrane. The membrane, which now experiences no stress, relaxes back to an unperturbed state.

The structure of the N-BAR domain of members of the endophilin family is unique because of the presence of the extra appendage Q59−Q88. The crystallographic structure of this region is partially missing, and information about its role in membrane binding and bending is derived largely from molecular modeling (*38*). It is believed to fold upon contact with the membrane and insert into the outer leaflet of the membrane (*14*). Evidence of this insertion has been provided recently (*18*). To understand the role of the appendage, two mutants (A66D and A66W) were examined. A66 is one of the conserved hydrophobic residues in the ridge. The A66D mutant could not tubulate the bilayer, and surprisingly, most of it bound to the mica substrate. This result indicates that introduction of a negative charge abolishes prolonged contact with the membrane over the observed time scale. A66W, on the other hand, caused tubulation and vesiculation. It has been previously shown that the bulky tryptophan residue is in a highly hydrophobic region (*14*), suggesting that it acts like a wedge between the two bilayer leaflets, driving vesiculation (*39*) (reviewed in ref *40*). Both these observations are consistent with a model in which the appendage is necessary for increased membrane contact, and generation of membrane curvature.

Our observations provide experimental evidence of some features of the proposed models of the endophilin N-BAR domain action. This study is also the first to be conducted on planar lipid bilayers instead of lipid vesicles. By following the action of the N-BAR domain under near-physiological conditions, and visualizing the process of bilayer sculpting stage by stage, we have been able to provide additional insights into the membrane binding and bending mechanism of the endophilin N-BAR domain.

ACKNOWLEDGMENT

We thank Dr. J. Bai (Department of Molecular Biology, Massachusetts General Hospital, Boston, MA) for providing the endophilin N-BAR domain constructs and for helpful comments about the manuscript.

REFERENCES

1. Brodin, L., Low, P., and Shupliakov, O. (2000) Sequential steps in clathrin-mediated synaptic vesicle endocytosis. *Curr. Opin. Neurobiol. 10*, 312–320.
2. Murthy, V. N., and De Camilli, P. (2003) Cell biology of the presynaptic terminal. *Annu. Rev. Neurosci. 26*, 701–728.
3. Reutens, A. T., and Begley, C. G. (2002) Endophilin-1: A multifunctional protein. *Int. Biochem. Cell Biol. 34*, 1173–1177.
4. Rikhy, R., Kumar, V., Mittal, R., and Krishnan, K. S. (2002) Endophilin is critically required for synapse formation and function in *Drosophila melanogaster*. *J. Neurosci. 22*, 7478–7484.
5. Verstreken, P., Kjaerulff, O., Lloyd, T. E., Atkinson, R., Zhou, Y., Meinertzhagen, I. A., and Bellen, H. J. (2002) Endophilin mutations block clathrin-mediated endocytosis but not neurotransmitter release. *Cell 109*, 101–112.
6. Verstreken, P., Koh, T. W., Schulze, K. L., Zhai, R. G., Hiesinger, P. R., Zhou, Y., Mehta, S. Q., Cao, Y., Roos, J., and Bellen, H. J.

(2003) Synaptojanin is recruited by endophilin to promote synaptic vesicle uncoating. *Neuron 40*, 733–748.
7. Ringstad, N., Gad, H., Low, P., Di Paolo, G., Brodin, L., Shupliakov, O., and De Camilli, P. (1999) Endophilin/SH3p4 is required for the transition from early to late stages in clathrin-mediated synaptic vesicle endocytosis. *Neuron 24*, 143–154.
8. Peter, B. J., Kent, H. M., Mills, I. G., Vallis, Y., Butler, P. J., Evans, P. R., and McMahon, H. T. (2004) BAR domains as sensors of membrane curvature: The amphiphysin BAR structure. *Science 303*, 495–499.
9. Giachino, C., Lantelme, E., Lanzetti, L., Saccone, S., Bella Valle, G., and Migone, N. (1997) A novel SH3-containing human gene family preferentially expressed in the central nervous system. *Genomics 41*, 427–434.
10. Ringstad, N., Nemoto, Y., and De Camilli, P. (1997) The SH3p4/Sh3p8/SH3p13 protein family: Binding partners for synaptojanin and dynamin via a Grb2-like Src homology 3 domain. *Proc. Natl. Acad. Sci. U.S.A. 94*, 8569–8574.
11. Sakamuro, D., Elliott, K. J., Wechsler-Reya, R., and Prendergast, G. C. (1996) BIN1 is a novel MYC-interacting protein with features of a tumour suppressor. *Nat. Genet. 14*, 69–77.
12. Farsad, K., Ringstad, N., Takei, K., Floyd, S. R., Rose, K., and De Camilli, P. (2001) Generation of high curvature membranes mediated by direct endophilin bilayer interactions. *J. Cell Biol. 155*, 193–200.
13. Weissenhorn, W. (2005) Crystal structure of the endophilin-A1 BAR domain. *J. Mol. Biol. 351*, 653–661.
14. Masuda, M., Takeda, S., Sone, M., Ohki, T., Mori, H., Kamioka, Y., and Mochizuki, N. (2006) Endophilin BAR domain drives membrane curvature by two newly identified structure-based mechanisms. *EMBO J. 25*, 2889–2897.
15. Gallop, J. L., Jao, C. C., Kent, H. M., Butler, P. J., Evans, P. R., Langen, R., and McMahon, H. T. (2006) Mechanism of endophilin N-BAR domain-mediated membrane curvature. *EMBO J. 25*, 2898–2910.
16. Cestra, G., Castagnoli, L., Dente, L., Minenkova, O., Petrelli, A., Migone, N., Hoffmuller, U., Schneider-Mergener, J., and Cesareni, G. (1999) The SH3 domains of endophilin and amphiphysin bind to the proline-rich region of synaptojanin 1 at distinct sites that display an unconventional binding specificity. *J. Biol. Chem. 274*, 32001–32007.
17. Schuske, K. R., Richmond, J. E., Matthies, D. S., Davis, W. S., Runz, S., Rube, D. A., van der Bliek, A. M., and Jorgensen, E. M. (2003) Endophilin is required for synaptic vesicle endocytosis by localizing synaptojanin. *Neuron 40*, 749–762.
18. Jao, C., Hegde, B. G., Gallop, J. L., Hegde, P. B., McMahon, H. T., Haworth, I. S., and Langen, R. (2010) Roles of amphipathic helices and the BAR domain of endophilin in membrane curvature generation. *J. Biol. Chem.* (in press).
19. Chen, Y., Deng, L., Maeno-Hikichi, Y., Lai, M., Chang, S., Chen, G., and Zhang, J. F. (2003) Formation of an endophilin-Ca^{2+} channel complex is critical for clathrin-mediated synaptic vesicle endocytosis. *Cell 115*, 37–48.
20. Lawrence, J. C., Saslowsky, D. E., Edwardson, J. M., and Henderson, R. M. (2003) Real-time analysis of the effects of cholesterol on lipid raft behavior using atomic force microscopy. *Biophys. J. 84*, 1827–1832.
21. Saslowsky, D. E., Lawrence, J., Ren, X., Brown, D. A., Henderson, R. M., and Edwardson, J. M. (2002) Placental alkaline phosphatase is efficiently targeted to rafts in supported lipid bilayers. *J. Biol. Chem. 277*, 26966–26970.
22. Shahin, V., Datta, D., Hui, E., Henderson, R. M., Chapman, E. R., and Edwardson, J. M. (2008) Synaptotagmin perturbs the structure of phospholipid bilayers. *Biochemistry 47*, 2143–2152.
23. Barrera, N. P., Ormond, S. J., Henderson, R. M., Murrell-Lagnado, R. D., and Edwardson, J. M. (2005) Atomic force microscopy imaging demonstrates that P2X2 receptors are trimers but that P2X6 receptor subunits do not oligomerize. *J. Biol. Chem. 280*, 10759–10765.
24. Neaves, K. J., Cooper, L. P., White, J. H., Carnally, S. M., Dryden, D. T. F., Edwardson, J. M., and Henderson, R. M. (2009) Atomic force microscopy of the EcoKI type I DNA restriction enzyme bound to DNA shows enzyme dimerisation and DNA looping. *Nucleic Acids Res. 37*, 2053–2063.
25. Schneider, S. W., Lärmer, J., Henderson, R. M., and Oberleithner, H. (1998) Molecular weights of individual proteins correlate with molecular volumes measured by atomic force microscopy. *Pfluegers Arch. 435*, 362–367.
26. Sprong, H., van der Sluijs, P., and van Meer, G. (2001) How proteins move lipids and lipids move proteins. *Nat. Rev. Mol. Cell Biol. 2*, 504–513.
27. Ludtke, S., He, K., and Huang, H. (1995) Membrane thinning caused by magainin 2. *Biochemistry 34*, 16764–16769.
28. He, K., Ludtke, S. J., Heller, W. T., and Huang, H. W. (1996) Mechanism of alamethicin insertion into lipid bilayers. *Biophys. J. 71*, 2669–2679.
29. Pabst, G., Danner, S., Podgornik, R., and Katsaras, J. (2007) Entropy-driven softening of fluid lipid bilayers by alamethicin. *Langmuir 23*, 11705–11711.
30. Mecke, A., Lee, D. K., Ramamoorthy, A., Orr, B. G., and Banaszak Holl, M. M. (2005) Membrane thinning due to antimicrobial peptide binding: An atomic force microscopy study of MSI-78 in lipid bilayers. *Biophys. J. 89*, 4043–4050.
31. Fernandes, F., Loura, L. M., Chichon, F. J., Carrascosa, J. L., Fedorov, A., and Prieto, M. (2008) Role of helix 0 of the N-BAR domain in membrane curvature generation. *Biophys. J. 94*, 3065–3073.
32. Ayton, G. S., Blood, P. D., and Voth, G. A. (2007) Membrane remodeling from N-BAR domain interactions: Insights from multi-scale simulation. *Biophys. J. 92*, 3595–3602.
33. Ayton, G. S., Lyman, E., Krishna, V., Swenson, R. D., Mim, C., Unger, V. M., and Voth, G. A. (2009) New insights into BAR domain-induced membrane remodeling. *Biophys. J. 97*, 1616–1625.
34. Blood, P. D., and Voth, G. A. (2006) Direct observation of Bin/amphiphysin/Rvs (BAR) domain-induced membrane curvature by means of molecular dynamics simulations. *Proc. Natl. Acad. Sci. U.S.A. 103*, 15068–15072.
35. Arkhipov, A., Yin, Y., and Schulten, K. (2008) Four-scale description of membrane sculpting by BAR domains. *Biophys. J. 95*, 2806–2821.
36. Yin, Y., Arkhipov, A., and Schulten, K. (2009) Simulations of membrane tubulation by lattices of amphiphysin N-BAR domains. *Structure 17*, 882–892.
37. Frost, A., Perera, R., Roux, A., Spasov, K., Destaing, O., Egelman, E. H., De Camilli, P., and Unger, V. M. (2008) Structural basis of membrane invagination by F-BAR domains. *Cell 132*, 807–817.
38. Cui, H., Ayton, G. S., and Voth, G. A. (2009) Membrane binding by the endophilin N-BAR domain. *Biophys. J. 97*, 2746–2753.
39. Campelo, F., McMahon, H. T., and Kozlov, M. M. (2008) The hydrophobic insertion mechanism of membrane curvature generation by proteins. *Biophys. J. 95*, 2325–2339.
40. Zimmerberg, J., and Kozlov, M. M. (2006) How proteins produce cellular membrane curvature. *Nat. Rev. Mol. Cell Biol. 7*, 9–19.